Science AAAS

Nanoscale Three-Dimensional Patterning of Molecular Resists by Scanning Probes

David Pires, *et al.*

Science **328**, 732 (2010);
DOI: 10.1126/science.1187851

This copy is for your personal, non-commercial use only.

If you wish to distribute this article to others, you can order high-quality copies for your colleagues, clients, or customers by clicking here.

Permission to republish or repurpose articles or portions of articles can be obtained by following the guidelines here.

The following resources related to this article are available online at www.sciencemag.org (this information is current as of May 10, 2010):

Updated information and services, including high-resolution figures, can be found in the online version of this article at:
http://www.sciencemag.org/cgi/content/full/328/5979/732

Supporting Online Material can be found at:
http://www.sciencemag.org/cgi/content/full/science.1187851/DC1

This article appears in the following **subject collections**:
Materials Science
http://www.sciencemag.org/cgi/collection/mat_sci

Downloaded from www.sciencemag.org on May 10, 2010

Science (print ISSN 0036-8075; online ISSN 1095-9203) is published weekly, except the last week in December, by the American Association for the Advancement of Science, 1200 New York Avenue NW, Washington, DC 20005. Copyright 2010 by the American Association for the Advancement of Science; all rights reserved. The title *Science* is a registered trademark of AAAS.

to the bosonic hard-sphere calculation $B = 8.5$ (*20*) and to the value $B \approx 7.2$ for point-like bosons with large scattering length (*19*).

Our measurements also allow direct comparison with advanced many-body theories developed for homogeneous gases in the strongly correlated regime. As displayed in Fig. 3A, our data are in agreement with a Nozières-Schmitt-Rink approximation (*21*) but show significant differences from a quantum Monte-Carlo calculation (*22*) and a diagrammatic approach (*23*). The measured EoS strongly disfavors the prediction of BCS mean-field theory.

Comparison with Fixed-Node Monte-Carlo theories requires the calculation of the EoS $\xi(1/k_F a)$ in the canonical ensemble

$$\xi\left(\frac{1}{k_F a}\right) \equiv \frac{E - \frac{N}{2}E_b}{\frac{3}{5}NE_F} \qquad (7)$$

that is deduced from $h_S^{\rm BCS}(\tilde{\delta})$ and $h_S^{\rm BEC}(\tilde{\delta})$ (*6*). As shown in Fig. 3B, the agreement with theories (*24–26*) is very good.

We now discuss the EoS of the partially polarized normal phase (black points in Fig. 1). At low concentrations, we expect the minority atoms to behave as noninteracting quasiparticles, the fermionic polarons (*27*). The polarons are dressed by the majority Fermi sea through a renormalized chemical potential $\mu_2 - A(\delta_1)\mu_1$ (*28*) and an effective mass $m^*(\delta_1)$ (*26*, *29*, *30*). Following a Fermi liquid picture, we propose to express the gas pressure as the sum of the Fermi pressure of the bare majority atoms and of the polarons (*4*).

$$h(\delta_1, \eta) = 1 + \left(\frac{m^*(\delta_1)}{m}\right)^{3/2} (\eta - A(\delta_1))^{5/2} \qquad (8)$$

Our measured EoS agrees with this model at unitarity and on the BEC side of the resonance (Fig. 1), where for $m^*(\delta_1)$ we use the calculations from (*30*, *31*). On the BCS side of the resonance, however, we observe at large minority concentrations an intriguing deviation to Eq. 8. In the BCS regime, the superfluid is less robust to spin imbalance. Consequently, the ratio of the two densities n_1/n_2 in the normal phase becomes close to unity near the superfluid/normal boundary η_c. The polaron ideal gas picture then fails.

Alternatively, we can let the effective mass m^* be a free parameter in the model in Eq. 8 in the fit of our data around $\eta = A$. We obtain the value of the polaron effective mass in the BEC-BCS crossover (Fig. 4).

An important consistency check of our study is provided by the comparison between our direct measurements of $\eta_c(\delta_1)$ (from Fig. 1, black dots in the inset of Fig. 4) and a calculated $\eta_c(\delta_1)$ from Eq. 8 and the EoS of the superfluid h_S. Assuming negligible surface tension, the normal/superfluid boundary is given by equating the pressure and chemical potential in the two phases. This procedure leads to the solid red line in the inset of Fig. 4, in excellent agreement with the direct measurements. In addition, by integrating our measured EoS of the homogeneous gas over the trap, one retrieves the critical polarization for superfluidity of a trapped gas, in agreement with most previous measurements (*6*).

We have measured the equation of state of a two-component Fermi gas at zero temperature in the BEC-BCS crossover. Extensions of our work include exploring the thermodynamics of the far BEC region of the phase diagram where a new phase associated with a polarized superfluid appears (*17*, *26*), mapping the EoS as a function of temperature, and investigating the influence of finite interaction range, which is playing a key role in higher-density parts of neutron stars.

References and Notes

1. M. Inguscio, W. Ketterle, C. Salomon, Eds. *Ultra-cold Fermi Gases: Proceedings of the International School of Physics "Enrico Fermi", Course CLXIV, Varenna, 20 to 30 June 2006* (IOS Press, Amsterdam, 2008).
2. A. J. Leggett, in *Modern Trends in the Theory of Condensed Matter*, A. Pekalski, R. Przystawa, Eds. (Springer-Verlag, Berlin, 1980), pp. 13–27.
3. Y. Shin, *Phys. Rev. A* **77**, 041603 (2008).
4. S. Nascimbène, N. Navon, K. J. Jiang, F. Chevy, C. Salomon, *Nature* **463**, 1057 (2010).
5. T. Ho, Q. Zhou, *Nat. Phys.* **6**, 131 (2009).
6. Materials and methods are available as supporting material on *Science* Online.
7. S. Nascimbène *et al.*, *Phys. Rev. Lett.* **103**, 170402 (2009).
8. Y. Shin, M. Zwierlein, C. Schunck, A. Schirotzek, W. Ketterle, *Phys. Rev. Lett.* **97**, 30401 (2006).
9. T. D. Lee, C. N. Yang, *Phys. Rev.* **105**, 1119 (1957).
10. R. B. Diener, R. Sensarma, M. Randeria, *Phys. Rev. A* **77**, 023626 (2008).
11. G. Baker Jr., *Rev. Mod. Phys.* **43**, 479 (1971).
12. H. Hu *et al.*, "Universal structure of a strongly interacting Fermi superfluid," http://arxiv.org/abs/1001.3200 (2010).
13. C. Lobo, I. Carusotto, S. Giorgini, A. Recati, S. Stringari, *Phys. Rev. Lett.* **97**, 100405 (2006).
14. S. Tan, *Ann. Phys.* **323**, 2971 (2008).
15. X. Leyronas, R. Combescot, *Phys. Rev. Lett.* **99**, 170402 (2007).
16. A. Altmeyer *et al.*, *Phys. Rev. Lett.* **98**, 040401 (2007).
17. Y. I. Shin, A. Schirotzek, C. H. Schunck, W. Ketterle, *Phys. Rev. Lett.* **101**, 070404 (2008).
18. T. Wu, *Phys. Rev.* **115**, 1390 (1959).
19. E. Braaten, H. W. Hammer, T. Mehen, *Phys. Rev. Lett.* **88**, 040401 (2002).
20. S. Tan, *Phys. Rev. A* **78**, 013636 (2008).
21. H. Hu, X. Liu, P. Drummond, *Europhys. Lett.* **74**, 574 (2006).
22. A. Bulgac, J. Drut, P. Magierski, *Phys. Rev. A* **78**, 023625 (2008).
23. R. Haussmann, W. Rantner, S. Cerrito, W. Zwerger, *Phys. Rev. A* **75**, 023610 (2007).
24. S. Chang, V. Pandharipande, J. Carlson, K. Schmidt, *Phys. Rev. A* **70**, 043602 (2004).
25. G. E. Astrakharchik, J. Boronat, J. Casulleras, A. S. Giorgini, *Phys. Rev. Lett.* **93**, 200404 (2004).
26. S. Pilati, S. Giorgini, *Phys. Rev. Lett.* **100**, 030401 (2008).
27. C. Lobo, A. Recati, S. Giorgini, S. Stringari, *Phys. Rev. Lett.* **97**, 200403 (2006).
28. A. Schirotzek, C.-H. Wu, A. Sommer, M. W. Zwierlein, *Phys. Rev. Lett.* **102**, 230402 (2009).
29. R. Combescot, A. Recati, C. Lobo, F. Chevy, *Phys. Rev. Lett.* **98**, 180402 (2007).
30. N. Prokof'ev, B. Svistunov, *Phys. Rev. B* **77**, 020408 (2008).
31. R. Combescot, S. Giraud, X. Leyronas, *Europhys. Lett.* **88**, 60007 (2009).
32. In the BEC limit, the grand-canonical EoS expands as $h_S(\tilde{\delta}) \cong 15\pi a/4a_{dd}\tilde{\delta} - 16\sqrt{2}$; the first term is the mean-field interaction and the second is the LHY correction asymptotic behavior.
33. A. Schirotzek, Y. I. Shin, C. H. Schunck, W. Ketterle, *Phys. Rev. Lett.* **101**, 140403 (2008).

34. We thank K. Jiang for participation in the early phase of the experimental work. We are grateful to X. Leyronas, C. Mora, Y. Castin, F. Werner, R. Combescot, J. Dalibard, F. Gerbier, and G. Shlyapnikov for stimulating discussions and critical comments on the manuscript. We thank S. Giorgini, P. Drummond, J. Drut, R. Haussmann, and W. Zwerger for providing us with their data. We acknowledge support from European Research Council, European Science Foundation (Euroquam), SCALA (Scalable Quantum Computing with Light and Atoms), Agence Nationale de la Recherche FABIOLA (Fermions and Bosons in Optical Lattices), Région Ile de France Institut Francilien de Recherche sur les Atomes Froids, and Institut Universitaire de France.

Supporting Online Material

www.sciencemag.org/cgi/content/full/science.1187582/DC1
Materials and Methods
Figs. S1 to S4
References

27 January 2010; accepted 30 March 2010
Published online 15 April 2010;
10.1126/science.1187582
Include this information when citing this paper.

Nanoscale Three-Dimensional Patterning of Molecular Resists by Scanning Probes

David Pires,[1] James L. Hedrick,[2] Anuja De Silva,[3] Jane Frommer,[2] Bernd Gotsmann,[1] Heiko Wolf,[1] Michel Despont,[1] Urs Duerig,[1] Armin W. Knoll[1]*

For patterning organic resists, optical and electron beam lithography are the most established methods; however, at resolutions below 30 nanometers, inherent problems result from unwanted exposure of the resist in nearby areas. We present a scanning probe lithography method based on the local desorption of a glassy organic resist by a heatable probe. We demonstrate patterning at a half pitch down to 15 nanometers without proximity corrections and with throughputs approaching those of Gaussian electron beam lithography at similar resolution. These patterns can be transferred to other substrates, and material can be removed in successive steps in order to fabricate complex three-dimensional structures.

To date, a wide variety of techniques has been available for nanofabrication (*1*), including electron beam lithography (EBL) and scanning probe lithography (SPL) (*2–4*) as direct-write methods. Although EBL is used in critical applications such as the fabrication of

Downloaded from www.sciencemag.org on May 10, 2010

masks for optical lithography (5), the fabrication of patterns at resolutions below 30 nm with EBL is difficult because of proximity effects (6). The throughput also scales unfavorably as the resolution is increased (7–9). Scanned probes are inherently capable of addressing surfaces with subnanometer precision. This capability has been exploited to create patterns with atomic resolution with a scanning tunneling microscope (STM) (10), albeit at extremely low patterning speeds.

In SPL, the close proximity of the tip to the substrate opens up multiple ways to modify the sample by the tip at resolutions below 50 nm (2–4). We demonstrate the use of a heated tip to locally desorb material from a thin film of an organic molecular glass. Structuring of organic materials as resists is our preferred strategy, because it follows the same philosophy as wafer-scale lithography methods in complementary metal-oxide semiconductor technology and enables the transfer of the pattern into arbitrary underlying substrates (e.g., by etching techniques). The approach avoids large stresses on the tip, such as are needed for plowing (11) or ultrasonic removal of material (12), and also mitigates the problem of piling up of excess material inherent in these approaches. Moreover, it does not require a conductive substrate in close proximity to the tip, as is necessary for current-induced depolymerization (13), field-induced deposition (14, 15), or field emission from the tip (16, 17).

Heated tips have already been used for patterning resists by removing covalently bound material (18, 19) and by inducing local chemical modifications (20, 21). However, cleavage of a chemical bond by a heated tip at very fast time scales is difficult because of the large energetic barriers of covalent bonds. Instead, we chose a resist material in which organic molecules are bound by hydrogen-bonding interactions into a glassy bulk state. The H bonds provide sufficient stability to the material for imaging and processing, but are sufficiently weak to be efficiently thermally activated by the hot tip.

The molecular structure of the resist used here is shown in Fig. 1C (22). Similar molecules have been designed as high-resolution photoresists (23, 22), and their relatively low molecular weight enables physical vapor deposition (PVD) of the material (24). The material under study has a molecular weight of 715 g/mol and a PVD temperature of ~220°C. Six hydroxy groups are located at the periphery of the molecule and give rise to numerous hydrogen-bonding interactions in the bulk of the material, as inferred from the high glass transition temperature T_g of 126°C.

The patterning principle (25) is shown in Fig. 1, A and B. The structure to be written was defined by a pixel set. At each pixel of the programmed pattern (red outline in Fig. 1, A and B), a force and a temperature stimulus were applied to the cantilever, which pulled the tip into contact from its rest position of ~300 nm above the surface (Fig. 1A) and induced the evaporation of a controlled amount of organic material (Fig. 1B). The heat and the force stimuli were provided by voltage pulses V_h and V_f, applied to a resistive heater coupled to the tip and to the substrate for electrostatic actuation, respectively. For a given interaction time (i.e., pulse duration), the depth of a written pixel depended on the applied force and temperature, as shown in Fig. 1D for pulse durations of 5.5 μs. The temperature given refers to the heater temperature T_{heater}. The actual increase relative to room temperature (RT) in resist temperature below the tip apex was ($T_{resist} - RT$) ≈ 0.4 to 0.5 ($T_{heater} - RT$) (26).

Two temperature regimes could be identified that were separated by a marked change in the sensitivity of pixel formation on the applied force. Below a threshold of ~330°C, the force-temperature characteristics were as expected for hot embossing (26, 27). For a given indent depth, the graphs are linear and converge to a common intersection point at ~350°C, as expected for a material with a T_g of 126°C (18). The indentation characteristics changed drastically if a heater temperature greater than ~330°C was applied. This transition marks the softening temperature of the material at a microsecond time scale and the crossover from an embossing regime to a regime of effective material removal (Fig. 1D). Above this threshold, sufficient thermal energy is provided to the material for breaking the hydrogen bonds at the microsecond time scale, allowing the molecular constituents to become mobile and escape from the surface. Experimental evidence supports a model in which the molecules diffuse along the tip into hotter tip regions, where the molecules are evaporated into the environment (25).

Figure 2 summarizes the results achieved using the patterning process. For the pattern shown in Fig. 2A, a total of 3.6×10^4 pixels were written at a pitch of 29 nm, resulting in uniformly recessed structures of 8 ± 1 nm depth, as evidenced by the depth histogram shown in Fig. 2C. The quality and uniformity of the patterning process can be seen in Fig. 2B and fig. S4. Each pixel of the programmed pattern, indicated by the red line, is well resolved. The depth of the pixels

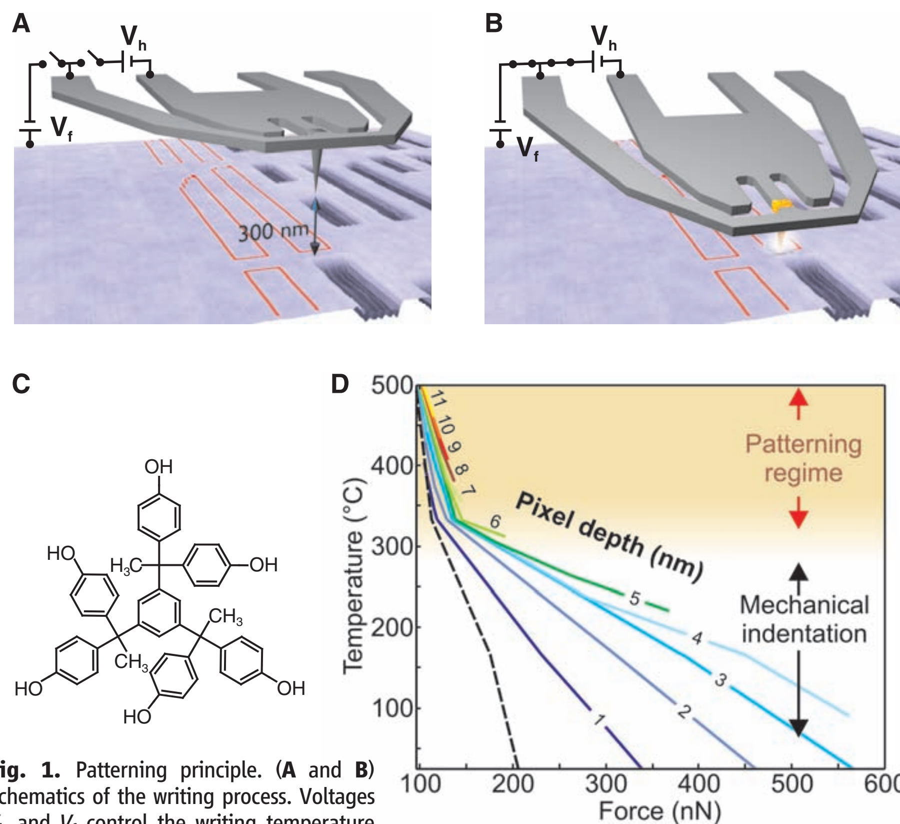

Fig. 1. Patterning principle. (**A** and **B**) Schematics of the writing process. Voltages V_h and V_f control the writing temperature and the electrostatic force, respectively. If no voltage is applied (A), the tip rests 300 nm above the surface. A pixel in the programmed bitmap (red outline) is written by simultaneously applying a force and temperature pulse for several microseconds. The force pulse pulls the tip into contact while the heat pulse heats the tip and triggers the patterning process. (**C**) Molecular structure of the phenolic compound used as resist. (**D**) Equi-depth lines of the pixels created in the resist upon single exposure events as a function of applied temperature and force. The dashed line indicates the writing threshold, determined by extrapolation to zero depth. Two regimes are separated by a threshold temperature of ~330°C. Below the threshold, the resist is mechanically deformed; above the threshold, it is efficiently removed.

[1]IBM Research–Zurich, Säumerstrasse 4, 8803 Rüschlikon, Switzerland. [2]IBM Research–Almaden, 650 Harry Road, San Jose, CA 95120, USA. [3]IBM Research–Watson, T. J. Watson Research Center, Yorktown Heights, NY 10598, USA.

*To whom correspondence should be addressed. E-mail: ark@zurich.ibm.com

Downloaded from www.sciencemag.org on May 10, 2010

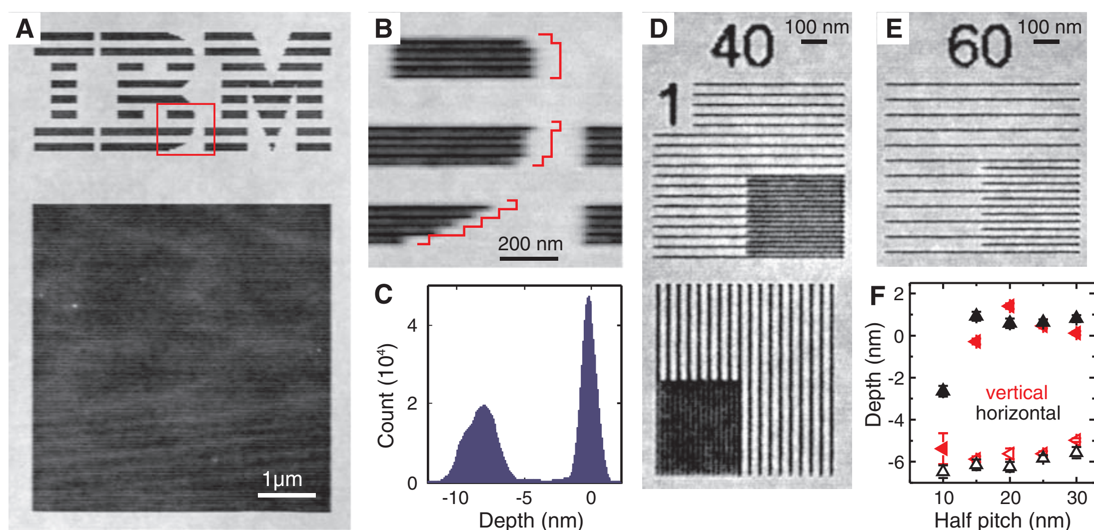

Fig. 2. Patterning of the molecular glass resist. (**A**) Topographic image of a pattern written into the molecular glass resist using a pixel size of 29 nm. Force and heat-pulse durations of 5.5 μs, a tip heater temperature of 300° ± 30°C, and a force of 80 ± 10 nN were applied for each pixel. (**B**) Close-up of the red box shown in (A), demonstrating the feature quality of the writing process. The red outline corresponds to the shape of the programmed image and is shifted relative to the real pattern for clarity. (**C**) Depth histogram of (A). The patterning depth is 8 ± 1 nm. (**D**) A field of dense lines at a line pitch of 40 nm written into a molecular glass film 20 ± 2 nm thick. One quadrant is written at half the line pitch (i.e., at 20 nm pitch). A pixel pitch of 10 nm, a tip heater temperature of 500° ± 30°C, and a force of 100 ± 10 nN were used. (**E**) Same as the top panel of (D) at a pitch of 60 nm (one quadrant is written at 30 nm pitch). (**F**) Depth of the written lines (open symbols) and height of the topography as measured between adjacent lines (solid symbols).

is the same regardless of the existence of written or unwritten neighboring pixels. In other words, at a pitch of 29 nm, proximity effects were absent. In the patterning process, a total volume of ~0.2 μm^3 was removed from the surface, which is more than 10^5 times that of the tip apex of ~1000 nm^3. However, no traces of displaced or redeposited material were detected either on the sample or at the tip. The efficiency of the process suggests that the molecules are removed without breaking covalent bonds and creating reactive species, which typically lead to tip contamination (*25*).

The achievable resolution increased with decreasing patterning depth. Figure 2, D to F, shows the result of high-resolution patterning at a depth of ~6 nm. A dense line pattern written at varying pitch was chosen to study the transition from single-line patterning to complete removal of material within a given area. For this experiment, pre- and post-heating of the tip for 2 and 3 μs, respectively, were applied at a force pulse duration of 5 μs to reduce thermal expansion and contraction of the cantilever structure during a patterning event. The average depth of the single lines and the average height of the topography between adjacent lines are shown in Fig. 2F. The error bars correspond to standard variations of the respective values. The depth of the lines has a constant value of ~6 nm, independent of the distance to neighboring lines. Down to a half pitch of 15 nm, the height of the topography between the lines was unaffected at the level of the unwritten resist surface; that is, any interference or proximity effects of neighboring lines were absent. Decreasing the half pitch further to 10 nm led to a reduction of the interline topography and enabled patterning of a flat, recessed area having a depth corresponding to the depth of the single lines (Fig. 2D). If we define the resolution of the process as the half pitch of fully separated dense lines, a resolution of ~15 nm was achieved using a tip with an apex radius of ~5 nm. The resolution can be further increased by using sharper tips or at the cost of a shallower pattern formation. In general, a finite value of the patterning depth is required to enable further processing—for example, for transferring the pattern into the underlying substrate or hard mask as described below.

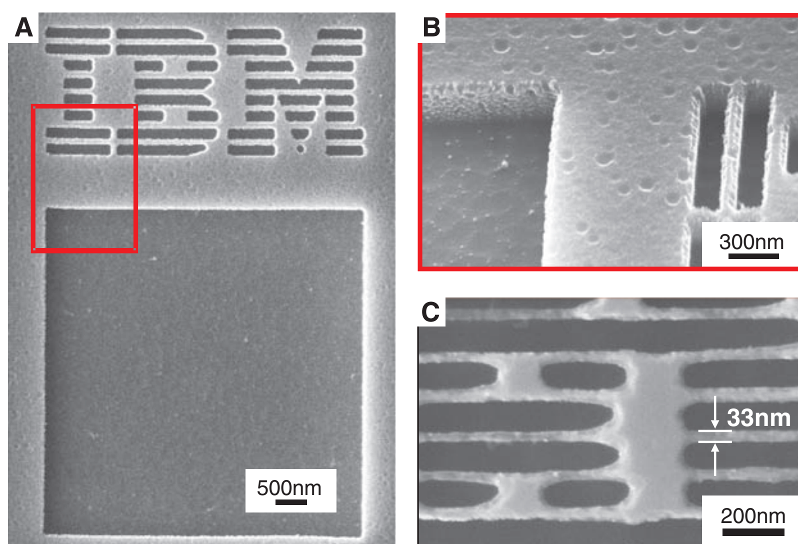

Fig. 3. Pattern transfer into silicon. (**A**) SEM image of the pattern shown in Fig. 2 transferred 400 nm deep into silicon. (**B**) Tilted view of the structure indicated by the red box in (A). (**C**) Zoom into a similar structure as shown in (A) but written at half the pixel pitch. The smallest lines fabricated in silicon had a width of ~30 nm.

For device fabrication, the structure depth in the target substrate must substantially exceed the depth of the patterns described above. For example, according to the International Technology Roadmap for Semiconductors, for the 22-nm node, a pattern in a resist 45 to 80 nm thick is required (*28*). A hard-mask strategy (*25*) has been adopted to amplify the pattern first into a resist layer of adequate thickness and subsequently into the silicon substrate. In short, the 8-nm-deep pattern within the molecular glass is first transferred into a 3-nm-thick silicon oxide hard mask by means of reactive ion etching (RIE). Subsequently, the hard mask serves as an etch-selective layer for the pattern transfer 70 nm deep into a poly(styrene-*r*-benzocyclobutene) (PS-BCB) (*29*) transfer layer.

At this stage, the required amplification into a thicker polymer layer was achieved, and different strategies could be implemented for further processing, such as deposition and liftoff of metal layers. Here we chose to transfer the pattern into the silicon substrate by another RIE process (*25*). Shown in Fig. 3, A and B, are

Downloaded from www.sciencemag.org on May 10, 2010

Fig. 4. Three-dimensional patterning. (**A**) AFM scan of the replica of the Matterhorn written into the molecular glass (3D data source: geodata © swisstopo). The structure was written using 120 steps of layer-by-layer removal. (**B**) Photograph of the Matterhorn in Switzerland (photographer: Marcel Wiesweg; source: Wikimedia). (**C**) AFM image of a Matterhorn replica transferred into silicon.

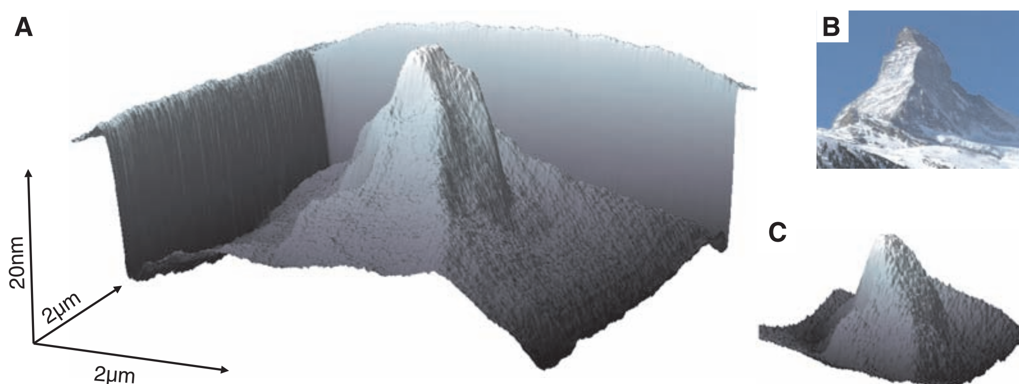

scanning electron microscopy (SEM) images of the final pattern in silicon as obtained after transfer of the pattern shown in Fig. 2A. The depth of the final structure in silicon is enhanced by a factor of 50 and amounts to more than 400 nm.

During the etch process, the pattern quality was maintained and only a fine rounding of the edges in the IBM logo was observed, caused by a slight over-etching. The large amplification enables the fabrication of high-aspect-ratio structures from the low-aspect-ratio SPL master. The same pattern as shown in Fig. 2A was written at half the pixel pitch (i.e., 15 nm), and a part of the final pattern in silicon is shown in Fig. 3C. The thickness of the walls between the patterned areas is 33 nm in the final silicon structure. As a result, vertical walls 33 nm thick and ~400 nm tall were fabricated, corresponding to an aspect ratio of >10 (*30*).

Material removal can be done in stages so that three-dimensional structures can be fabricated, as shown in Fig. 4. A given three-dimensional structure is processed into the resist by removing successive layers of defined thickness from the same sample area. A pyramid was created (fig. S6) with linear side walls, sharp edges, and a pointed tip. It demonstrates that each patterning step is reproducible and independent of the already existing structures created in preceding steps. By exploiting these properties, highly detailed and complex shapes can be reproduced. We fabricated a nanoscale replica of the Swiss mountain Matterhorn (Fig. 4B) in a 100-nm-thick molecular glass film (Fig. 4A). The patterning was achieved in 120 steps, resulting in a structure 25 nm tall (see also movie S1). Fine details of the original are reproduced in the nanometer-scale replica. The conformal reproduction of the original proves that the final structure is a linear superposition of well-defined single patterning steps. The result of a direct transfer of a similar structure into the underlying substrate is shown in Fig. 4C. Using a mixture of SF_6 and C_4F_8 as etch gas provides a height amplification of the structures into silicon by a factor of ~3.

Areal throughputs in the range of 5×10^4 μm^2/hour are achievable today assuming a duty cycle of 50%, which is sufficient for rapid prototyping applications in nanotechnology and approaches the throughput of EBL at similar resolution (*7*). High parallelization of a similar process using the same levers has been developed for a thermomechanical probe data storage system (*31*), enabling a potential throughput enhancement proportional to the number of levers operated at the same time. Assuming 1000 levers in parallel leads to throughput numbers that cannot be achieved by any other direct-write technology to date at the same resolution. At the same time, the direct development method offers in situ inspection and, potentially, in situ repair of structures not fully reproduced. Proximity effects are absent at pixel dimensions of ~15 nm and higher. Therefore, no computationally elaborate, substrate-dependent adjustment of the exposure dose is needed. Moreover, the dry nature of the entire patterning process eliminates solvent-related problems such as swelling-induced instability or drying-induced collapse of dense structures. Furthermore, the ability to generate three-dimensional templates having a nanometer-precise profile is a complementary match to nanoimprint lithography (*32*).

References and Notes

1. Y. Xia, J. A. Rogers, K. E. Paul, G. M. Whitesides, *Chem. Rev.* **99**, 1823 (1999).
2. R. Garcia, R. V. Martinez, J. Martinez, *Chem. Soc. Rev.* **35**, 29 (2006).
3. A. A. Tseng, A. Notargiacomo, T. P. Chen, *J. Vac. Sci. Technol. B* **23**, 877 (2005).
4. D. Wouters, U. S. Schubert, *Angew. Chem. Int. Ed.* **43**, 2480 (2004).
5. H. J. Levinson, *Principles of Lithography* (SPIE–International Society for Optical Engineering, Bellingham, WA, 2005).
6. T. H. P. Chang, *J. Vac. Sci. Technol.* **12**, 1271 (1975).
7. C. R. K. Marrian, D. M. Tennant, *J. Vac. Sci. Technol. A* **21**, S207 (2003).
8. R. Menon, A. Patel, D. Gil, H. I. Smith, *Mater. Today* **8**, 26 (2005).
9. J. A. Liddle, G. M. Gallatin, L. E. Ocola, in *Three-Dimensional Nanoengineered Assemblies* (Materials Research Society Symposium Proceedings, vol. 739), T. M. Orlando, L. Merhari, K. Ikuta, D. P. Taylor, Eds. (Materials Research Society, Warrendale, PA, 2003), pp. 19–30
10. D. M. Eigler, E. K. Schweizer, *Nature* **344**, 524 (1990).
11. L. L. Sohn, R. L. Willett, *Appl. Phys. Lett.* **67**, 1552 (1995).
12. F. Iwata, T. Matsumoto, R. Ogawa, A. Sasaki, *J. Vac. Sci. Technol. B* **17**, 2452 (1999).
13. C. Martín, G. Rius, X. Borrisé, F. Pérez-Murano, *Nanotechnology* **16**, 1016 (2005).
14. R. V. Martínez, N. S. Losilla, J. Martinez, Y. Huttel, R. Garcia, *Nano Lett.* **7**, 1846 (2007).
15. M. Rolandi, I. Suez, A. Scholl, J. M. Frechet, *Angew. Chem. Int. Ed.* **46**, 7477 (2007).
16. S. W. Park, H. T. Soh, C. F. Quate, S. I. Park, *Appl. Phys. Lett.* **67**, 2415 (1995).
17. K. Wilder, C. F. Quate, B. Singh, D. F. Kyser, *J. Vac. Sci. Technol. B* **16**, 3864 (1998).
18. B. Gotsmann, U. Duerig, J. Frommer, C. J. Hawker, *Adv. Funct. Mater.* **16**, 1499 (2006).
19. A. A. Milner, K. Zhang, Y. Prior, *Nano Lett.* **8**, 2017 (2008).
20. O. Fenwick *et al.*, *Nat. Nanotechnol.* **4**, 664 (2009).
21. R. Szoszkiewicz *et al.*, *Nano Lett.* **7**, 1064 (2007).
22. A. De Silva *et al.*, *Chem. Mater.* **20**, 1606 (2008).
23. J. Dai, S. W. Chang, A. Hamad, N. Felix, C. K. Ober, *Chem. Mater.* **18**, 3404 (2006).
24. F. Pfeiffer, N. M. Felix, C. Neuber, C. K. Ober, H. W. Schmidt, *Adv. Funct. Mater.* **17**, 2336 (2007).
25. See supporting material on *Science* Online.
26. B. Gotsmann, M. A. Lantz, A. Knoll, U. Duerig, *Nanotechnology, Vol. 6: Nanoprobes* (VCH, Weinheim, Germany, 2009), pp. 121–169.
27. The resist temperature at a heater temperature of 350°C is ~170°C. The temperature difference from the glass transition temperature of T_g = 126°C is consistent with the time-temperature behavior of glassy organic materials. Preliminary experiments recoding the indent depth as a function of heater temperature and writing time reveal a decrease of the writing threshold temperature with increasing exposure duration by ~20°C per decade at microsecond time scales, leveling off at a heater temperature of ~250°C for writing times of seconds.
28. International Technology Roadmap for Semiconductors, 2008 Update (www.itrs.net/Links/2008ITRS/Update/2008Tables_FOCUS_B.xls).
29. E. Harth *et al.*, *J. Am. Chem. Soc.* **124**, 8653 (2002).
30. Because of the high aspect ratio, we could not measure the depth by atomic force microscopy (AFM). Therefore, we assume that the etch depth for these narrow trenches is similar to that for the large structures of 400 nm.
31. A. Pantazi *et al.*, *IBM J. Res. Develop.* **52**, 493 (2008).
32. K. Watanabe *et al.*, *J. Vac. Sci. Technol. B* **22**, 22 (2004).
33. We gratefully acknowledge the invaluable support from the probe storage team at the IBM Research Laboratory in Rüschlikon, in particular U. Drechsler for the pattern transfer and the fabrication of thermomechanical probe sensors, and P. Seidler, W. Riess, R. Miller, and R. Allen for stimulating discussions.

Supporting Online Material

www.sciencemag.org/cgi/content/full/science.1187851/DC1
Materials and Methods
SOM Text
Figs. S1 to S6
Movie S1

2 February 2010; accepted 30 March 2010
Published online 22 April 2010;
10.1126/science.1187851
Include this information when citing this paper.

Downloaded from www.sciencemag.org on May 10, 2010